ADVANCED MATERIALS INTERFACES
Open Access
www.advmatinterfaces.de



# Bioactive Salicylic Acid Containing Coating for Dental Implants to Combat Infection and Inflammation

*Yashoda Chandorkar,* Moritz Valeske, Barbora Kolrosova, Yvonne Elbs-Glatz, Flavia Zuber, Jean Schoeller, Nico Kummer, Qun Ren, Markus Rottmar, and Katharina Maniura-Weber**

**The long-term stability of dental implants depends on successful osseointegration and on the soft tissue interface seal formed between the implant and gingiva. This seal plays a pivotal role in blocking the entry of microorganisms, thereby preventing the onset of common implant-associated diseases, e.g., peri-implantitis. Bioactive coatings constitute a promising approach to modulate tissue response around dental implants but are associated with challenges in simultaneously achieving antimicrobial effects as well as controlling inflammation. This study reports a salicylic acid-based bioactive coating, which is facile to synthesize and can be easily applied on metallic surfaces like titanium. The local release of salicylic acid exhibits potent antibacterial activity against *Staphylococcus aureus* and modulates the immune response to coated surfaces by decreased expression of proinflammatory macrophage markers. The differentiation of fibroblasts into the myofibroblast phenotype, which is essential for wound healing due to their contractile properties is unaffected. The coating also displays antithrombogenic capabilities due to the anticoagulation property of salicylic acid; without negatively influencing mineralization of human bone progenitor cells. With salicylic acid being an inexpensive biomolecule, this bioactive coating represents a promising approach to improve the acceptance and function of dental implants and possibly other implant types.**

## 1. Introduction

Replacing missing teeth with dental implants is a very common and successful therapeutic approach. The prevalence is on the rise, with 800 000 and 1.8 Million dental implants being implanted annually in the US and in the EU, respectively.[1] However, the failure rates of dental implants are reported to be around 3% after 10 years and increase to 25% after 20 years of implantation, and hence efforts to develop more successful implants are strongly desired.[2,3] Peri-implant mucositis, which can progress to peri-implantitis, constitutes one of the most common complications (91.4% of all diseased dental implants)[4] that affects the hard and soft tissue surrounding the implant and if left untreated, it leads to implant loss.[5,6]

The attachment of soft tissue to the trans-mucosal part of the implant provides the first mechanical barrier to the entry of bacteria and bacterial toxins, and hence provides a protective function against bone resorption.[7] A compromised seal facilitates the entry of bacteria and microorganisms, diminishes good osseointegration, and contributes to implant failure through a complex host-mediated inflammatory response, eventually leading to loss of osseointegration.[2,8] The attachment of keratinocytes to the implant is necessary for a tight seal between the implant and the soft tissue surrounding the implant. However, in the presence of blood, where fibrin clots

Y. Chandorkar, M. Valeske, B. Kolrosova, Y. Elbs-Glatz, F. Zuber, Q. Ren, M. Rottmar, K. Maniura-Weber
Laboratory for Biointerfaces
Empa
Swiss Federal Laboratories for Materials Science and Technology
St Gallen 9014, Switzerland
E-mail: yashoda.chandorkar@empa.ch; katharina.maniura@empa.ch

The ORCID identification number(s) for the author(s) of this article can be found under https://doi.org/10.1002/admi.202300750



**DOI: 10.1002/admi.202300750**

J. Schoeller
Laboratory for Biomimetic Membranes and Textiles
Empa
Swiss Federal Laboratories for Materials Science and Technology
St Gallen 9014, Switzerland

N. Kummer
Laboratory for Cellulose & Wood Materials
Empa
Swiss Federal Laboratories for Materials Science and Technology
Dübendorf 8600, Switzerland

N. Kummer
Laboratory of Food Process Engineering
Institute of Food
Nutrition and Health
Department of Health Science and Technology
ETH Zürich
Zürich 8092, Switzerland

and fibrinogen are present, the adhesion of keratinocytes is prevented or very weak. This is due to the absence of integrin $\alpha_v\beta_3$ on keratinocytes, which is necessary to adhere to fibrinogen and fibrin.[9] Hence it is essential to create an implant surface conducive for keratinocyte attachment.

Bacterial colonization on the implant surface occurs within minutes/hours after implantation. An imbalance between bacterial load and the innate host defense that is activated when metallic implants are in contact with soft tissues marks the onset of peri-implantitis.[10–12] Later on, bacterial biofilms are thought to be the initial trigger for inflammatory responses, and initial bacterial colonizers act as substrates for successive colonizers in the process of biofilm formation.[8,12] Hence, for long-term implant survival, implant surfaces benefit from improvement in the prevention of primary adhesion of microbes and reduction of inflammation.

In the presence of certain factors such as the tumor growth factor $\beta$ (TGF-$\beta$) that are commonly associated with inflammation, fibroblasts undergo differentiation to myofibroblasts, which are contractile in nature, express $\alpha$-smooth muscle actin ($\alpha$SMA) and increase the synthesis of extracellular matrix (ECM) proteins such as collagens.[13] Contraction of wounds is an important function of myofibroblasts, since it results in wound closure and hence facilitates wound healing.[14] Different strategies involving organic chemistry-based coatings have been pursued to enhance the attachment of soft tissue to implants. One strategy includes coatings with ECM molecules that provide attachment sites for epithelial cells such as keratinocytes.[15] Another approach involves the prevention of peri-implant infection via the local release of antibiotics (e.g., gentamicin[16] ), however they have proven to be ineffective in treating severe peri-implantitis[17] and pose the risk of developing drug resistant bacteria. Antimicrobial peptides (such as GL13K[18] or LL37[19]), on the other hand are effective but expensive. Very few strategies that can combine several of the desired attributes such as supporting cell attachment, preventing bacterial attachment, promoting wound healing but at the same time preventing excessive host response exist. In one such strategy, cell adhesive peptides that promote keratinocyte attachment are combined with conjugated linoleic acid as an anti-inflammatory agent.[20] In another approach, a peptide that supports hemidesmosome formation by keratinocytes (LamLG3) was co-immobilized along with an anti-microbial peptide (GL13K) to improve the mechanical barrier at the tissue–implant interface and prevent bacterial infection.[21] Both these strategies are based on peptide sequences, which suffer from inactivity at physiological salt concentrations and susceptibility to proteases, apart from being expensive.

Salicylic acid (SA) is a very common nonsteroidal anti-inflammatory drug (NSAID) with antibacterial, antibiofilm formation, antipyretic, and anticoagulation properties,[22] and has also shown to reduce host response.[23] It is the deacetylation product of aspirin (acetylated salicylic acid), which is a non-prescription drug that is widely used for more than a century.[24] Compared to aspirin, which has a plasma half-life of 15 min, SA has a concentration-dependent half-life of 2–30 h.[25] As a result, the bioavailability of SA exceeds that of aspirin by a factor of 30 to 50.[26] At therapeutic concentrations linked to anti-inflammatory effects (a plasma concentration of 150–300 µg mL$^{-1}$), 80–90% of SA is bound to serum proteins.[27,28] This suggests that concentrations as low as 15–30 µg mL$^{-1}$ of free, unbound salicylate are present in serum. Consequently, higher systemic doses compared to local doses are necessary to achieve therapeutic concentrations, a drawback that can be avoided with local delivery by a coating.

Here we propose a simple and affordable strategy to improve implant acceptance through an SA-based coating that can i) prevent the initial attachment of bacteria and early implant colonization, ii) modulate inflammation and iii) modulate the wound environment by influencing blood interactions with the implant. We present a concept based on the incorporation of SA into the polymer backbone of the coating, which consists of ester and amide linkages that are labile and undergo hydrolysis. SA is incorporated in the oligomeric backbone to enable homogeneous release, and brittleness is avoided by low crosslinking density and the coating is facile, biologically active, easy to apply to metallic implants. After confirming the sequential layers of the coating by chemical and thickness characterization, we evaluate the efficacy of the coating with respect to its anti-bacterial activity against *Staphylococcus aureus*, immunomodulatory potential by evaluating macrophage polarization, effect on fibroblast and osteoblast differentiation and blood coagulation. The coating is intended for implant abutments that are in contact with the soft tissue, and hence, does not interfere with osseointegration. Our observations show that this concept holds great promise for the creation of a structural barrier seal between implant and soft tissue.

## 2. Experimental Section

### 2.1. Materials

All chemicals were obtained from Sigma-Aldrich, unless stated otherwise. Glass coverslips (diameter = 5 or 15 mm, thickness No 3, from Marienfeld) or Ti implants (machined, Type 4, kindly provided by Straumann AG) were used as substrates in this study.

### 2.2. Coating Rationale and Methodology

A bioinspired method was adopted that is based on the polydopamine (Pda) chemistry used by mussels to cling to wet surfaces (**Figure 1**, Step 1). SA is highly hydrophobic and has limited solubility in water (2.2 g L$^{-1}$). SA was conjugated on the terminal carboxylic groups of sebacic acid to form sebacic disalicylate, referred to as diacid throughout this manuscript (Figure 1, Step 2). A hydrophobic linker molecule such as sebacic acid was chosen since it is reported to influence properties such as polymer crystallinity and hence, provide control over the degradation. It is further approved by the US Food and Drug Administration for use in polymers for medical applications.[29,30] Sebacic acid is also a natural intermediate during $\omega$-oxidation of fatty acids, and hence, is safe in vivo.[31,32] In a second step, an oligomer was synthesized by the reaction of the diacid with glycerol, a polyol that is found naturally in lipids, through melt condensation (Figure 1, Step 3) and was spin coated on the Pda layer. This oligomer, soluble in organic solvents, was cured (thermally crosslinked) and referred

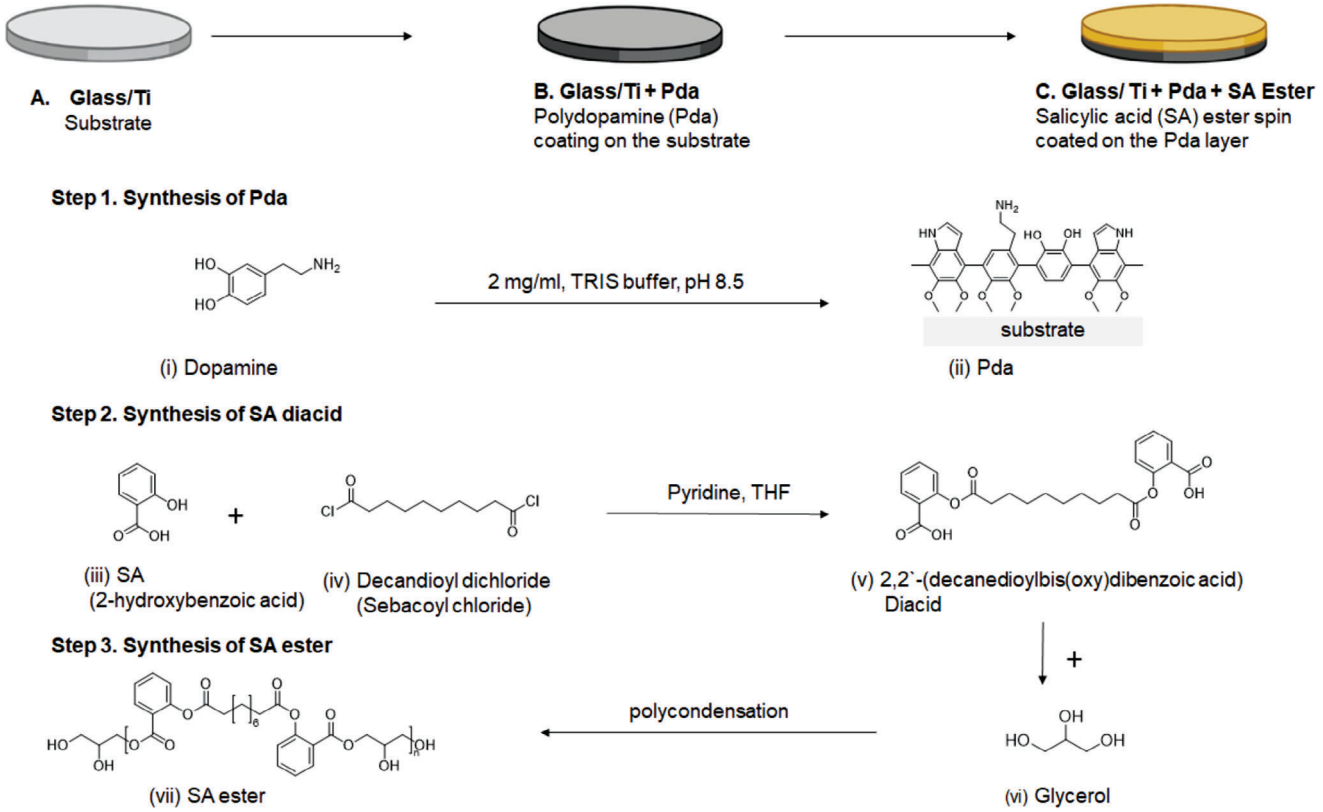


**Figure 1.** A schematic of the steps used to coat the substrates (Ti or glass, A) Step 1. The first step involves the synthesis of Pda, which forms a coating layer on the surface of the substrate that serves to connect the metallic/amorphous substrate with an organic molecule (Glass/Ti + Pda, B). Step 2. Sebacic acid capped with salicylic acid (SA) on both sides is synthesized and is then polymerized with glycerol to create a partially crosslinked molecule that is still soluble. This is used for spin coating the Pda coated substrate (B), which is followed by a curing step at 100 °C for 4 h to create Glass/Ti +Pda+ester (C). Created with BioRender.com.

to as the SA ester in the rest of the manuscript. Thus, a layer-by-layer sequential approach was adopted in which the SA ester is spin coated onto the Pda layer (**Figure 2**).

### 2.3. Synthesis

Salicylic acid based diacid: Diacid (Figure 1, structure (v)) was synthesized following previous procedures.[29] Salicylic acid (6 g, 43.44 mmol, 1 eq.) was dissolved in 45 mL pyridine and 15 mL THF. The reaction mixture was cooled to 0 °C. Sebacoyl chloride (5.19 g, 21.72 mmol, 4.633 mL, 0.5 eq.) was added dropwise to the stirred reaction mixture under nitrogen protection. The reaction was stirred for 3 h at room temperature. After 3 h the reaction was poured over crushed ice and water. This mixture was acidified with concentrated HCl to a pH value of 2. The reaction product was isolated with vacuum filtration and washed with MQ water with 18.2 MΩ cm resistivity (3 × 200 mL). The product was recrystallized from a water/acetone (9:1) mixture and dried under vacuum. The product was recovered as a white powder (6.76 g, 14.36 mmol, 66.12% yield) with a purity of 94%. This compound is referred to as the diacid in the manuscript. In this reaction, pyridine and tetrahydrofuran (THF) were used as solvents, since this combination prevented the formation of acyl pyridinium salt, and facilitated selective attack of the acyl pyridinium ion on the phenolate group.[33,34] In addition, the purification step involved precipitation of the diacid at low pH, and multiple washings with water, resulting in a purified diacid.[35] $^1$H NMR (400 MHz, $CDCl_3$) confirmed the structure and the following peaks were observed $\delta$ 8.16 (d, 2H, ArH), 7.64 (t, 2H, ArH), 7.37 (t, 2H, ArH), 7.15 (d, 2H, ArH), 2.65 (t, 4H, $CH_2$), 1.84 (m, 4H, $CH_2$), 1.48 (m, 8H, $CH_2$).

#### 2.3.1. Oligomer Formation

Diacid (v) (0.5 g, 1.13 mmol, 1 eq.) and glycerol 4 (69 mg, 0.75 mmol, 0.66 eq.) were mixed. The reaction was heated with a heat gun until the diacid had melted. In this molten state, the reagents were mixed with a spatula. After mixing the reaction was cured in the oven at 100 °C for 4 h. $^1$H NMR (400 MHz, $CDCl_3$) confirmed the structure and the following peaks were observed: $\delta$ 7.93 (d, 2H, ArH), 7.54 (t, 2H, ArH), 7.02 (d, 2H, ArH), 6.95 (t, 2H, ArH), 4.6–3.5(m, 9H, $CH_2$), 2.37 (m, 4H, $CH_2$), 1.66 (m, 4H, $CH_2$), 1.35 (m, 8H, $CH_2$).

#### 2.3.2. Coating of the Substrate with Polydopamine (Pda Coating)

The substrates were cleaned by ultrasonication using distilled water and isopropanol for 5 min each and then air dried. The

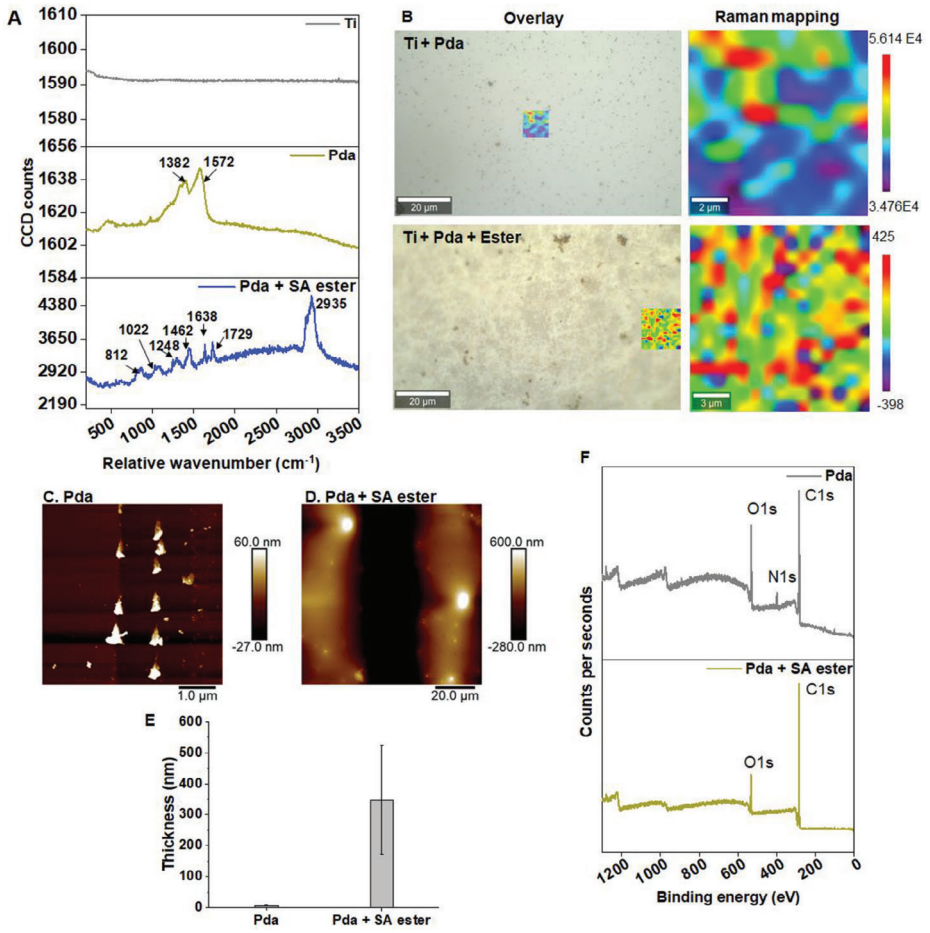


**Figure 2.** A) Confocal scanning Raman microscopy showing the presence of vibration peaks obtained in the Stokes mode for Ti, Ti + Pda and Ti + Pda + ester, B) brightfield image of Ti+ Pda with the mapped area, with an overlay of the brightfield image with a map generated from the Raman spectrum after applying a filter from 1338 $cm^{-1}$ to 1638 $cm^{-1}$ accounting for the dopamine bands (top row). Brightfield image of Ti + Pda + ester with an overlay of the map generated from the Raman spectrum after applying a filter from 1715 to 1745 $cm^{-1}$ for the C=O of SA for Pda + SA ester (Bottom row). C,D) Atomic force microscopy images (height sensor channel) showing the presence of a scratch that is created to determine the thickness of Si wafer coated with C) Pda and D) Pda + ester. E) Thickness of the coatings, determined as shown in (C,D). F) X-ray photoelectron spectroscopy showing the presence of nitrogen on the Pda coated Ti, which is not observed in the Ti+Pda + SA ester, showing that the SA ester completely covers the Pda surface.

substrates were treated with air plasma (Harrick Plasma Cleaner, 0.14 bar, 60s, 29.6 W power) and then immersed in a solution of 2 mg $mL^{-1}$ of dopamine hydrochloride (as reported earlier[36]) prepared in $10 \times 10^{-3}$ M TRIS buffer (pH 8.5) overnight at room temperature. The next day, the substrates were washed three times with distilled water to remove the dopamine flake deposition, followed by a wash with isopropanol, after which the samples were air-dried.

### 2.3.3. Spin Coating of SA-Ester (Pda + Ester)

A solution of 48 mg $mL^{-1}$ of the SA ester was prepared in methanol, and spin coated on the substrates using a spin coater (Laurell WS- 650 MZ-23NPPB model) at a speed of 2500 rpm for 30 s and 5000 rpm for 50 s. The pre-polymer solution (10 µL for diameter 5 mm, 50 µL for diameter 15 mm) was added to the substrate before spinning (static spin coating). Small diameter samples were glued on a glass slide. After spin coating, the samples were cured at 100 °C for 4 h in an oven to facilitate further polymerization.

### 2.3.4. Coupling with Diacid (Pda+ Diacid)

The SA diacid was attached to the dopamine coated substrates using carbonyldiimidazole (CDI), with a stoichiometry of 1:1. Dichloromethane (DCM) was used as the solvent and was in excess. The Pda coated substrates were immersed in a solution containing SA diacid:carbonyldiimidazol (CDI) in a molar stoichiometry ratio of 1:1, with dichloromethane (DCM) as the solvent. After 4 h of shaking such that the substrates did not flip, the substrates are washed with DCM three times, and air dried.

## 2.4. Raman Spectroscopy

Raman spectra were acquired using a Witec Alpha 300 Laser scanning confocal Raman spectrometer. Rayleigh scattering was

eliminated using a notch filter and Raman spectra from 0 to 3500 $cm^{-1}$ were acquired. The filtered light was scattered by one grating with 600 grooves $mm^{-1}$ and an electron multiplying charge coupled device (EM CCD) camera cooled at 213 K with 1600 × 200 pixel array, pixel size 16 × 16 µm was used for detection. The 532 nm line of the frequency doubled Nd:YAG laser was used for excitation, and spectra are recorded in Stokes mode (inelastic scattering). When single acquisition was not sufficient to give a good signal, area scans were recorded with a resolution of 1 line per µm and a speed of 0.1 sec per line. Data were averaged and cosmic ray radiation background was removed. For Raman spectroscopy machined Ti discs were polished prior to coating.

### 2.5. X-Ray Photoelectron Spectroscopy

X-ray photoelectron spectroscopy (XPS) measurements were performed using a Quantum 2000 X-ray photoelectron spectrometer (Physical Electronics, Minnesota, United States), equipped with an Al K$\alpha$ monochromatic source. Survey spectra were acquired at a pass energy of 117.4 eV (energy step of 1 eV). Elemental abundance was calculated by integrating the area under the curve (Table S1, Supporting Information).[36] The atomic fractions $x_a$ of a specific element was calculated from the survey scans using Equation 1:

$$x_a = \frac{\frac{I_a}{RSF_a}}{\sum_i \frac{I_i}{RSF_i}} \quad (1)$$

where the relative sensitivity factors (RSF) were obtained from the XPS software (Multipak) and Tougaard backgrounds were subtracted to measure the peak intensity ($I_i$) of each element.

### 2.6. Atomic Force Microscopy

AFM images of the different layers of the coating on silicon wafers were obtained using a Bruker Icon 3 microscope equipped with ScanAsyst probes and operated in the ScanAsyst mode. The lateral resolution of the images was 512 × 512 lines in a scan area determined by the scratch size and a scan rate of 0.5 Hz was maintained. To measure the thickness, a scratch was manually created on the coating (without scratching the Si-wafer) using a clean syringe needle. The thickness of the coating was determined from the height sensor image, using Bruker Nanoscope software. First-order smoothening was performed on the image after which the step function was used to calculate the thickness of the coating. Peak force error data were used to visualize the scratch due to better contrast visible in these images.

### 2.7. Contact Angle Measurement

The contact angle of different coating layers on polished Ti surfaces (grade 4) was measured with deionized water on a goniometer (Krüss). A drop of 2 µL was placed on the surface of the coating at a speed of 2.67 µL $s^{-1}$ and the contact angle at the solid–liquid interface was measured using Young-Laplace fitting. At least 6 values were determined on each coating at random positions

### 2.8. Measurement of Streaming Potential

The surface zeta potential or the streaming potential of the Pda and the Pda + diacid was measured using a SurPASS 3 device (Anton Paar, Graz Austria) that measures the zeta potential at the coating/electrolyte (0.001 M KCl) interface. An adjustable gap cell for planar samples was used with a gap size of 100 µm and the streaming potential of silicon wafers (2 × 2 cm) with the coating of interest was measured. pH scans from pH 3 to 8 were performed with 3 rinse cycles before each step.

### 2.9. Degradation of Coating and Release of SA

Estimation of SA released by the coating was performed using a Nanodrop one spectrophotometer (Thermo Scientific). For this, Pda+ ester and Pda + diacid + ester coated glass slides (diameter = 15 mm) were immersed in PBS (100 µL) for different time points, and 1.5 µL of this PBS was used to measure SA. A calibration curve was obtained with known amounts of SA (Figure S5D, Supporting Information).

### 2.10. Antimicrobial Activity

#### *2.10.1. Bacterial Culture*

*Staphylococcus aureus* (ATCC 6538) was the pathogen used in the antibacterial assay. Bacteria from glycerol stocks were grown on Tryptic Soy Agar (TSA) plates. One colony was transferred to 5 mL of 30% Tryptic Soy Broth supplemented with 0.25% glucose (TSB) and incubated overnight at 37 °C/160 rpm. Overnight culture was diluted to an OD 600 of 0.2 in 5 mL fresh TSB and again, cultivated for around 1.5–2 h until exponential growth. For final use on the coatings, the suspension was diluted to $10^5$ (OD600 0.001) colony forming units (CFU) $mL^{-1}$ in 0.9% NaCl. Therefrom, 50 µL of bacterial suspension was added to the sterilized samples in 12-well plates and incubated for 4 h at room temperature.

#### *2.10.2. Contact-Touch Test and Quantification*

After incubation of bacteria on the samples, the bacterial suspension was removed and the samples washed once with 200 µL of 0.9% NaCl. Thereafter, samples were placed on Plate-Count Agar and subsequently incubated for 30 s at room temperature to allow transfer of viable bacteria from samples onto agar. Finally, samples were removed and agar plates incubated at 37 °C for overnight. Agar plates with bacterial colonies were imaged by the use of a colony counter (Scan 300, Interscience, France). To quantify the colonies, after incubation, the samples were thoroughly washed twice with 200 µL of 0.9% NaCl. A serial dilution of the suspensions was performed in 0.9% NaCl until $10^{-3}$. Subsequently, 20 µL of each dilution was dropped and allowed to fully absorb on Plate-Count Agar in triplicates. All plates were incubated at 37 °C overnight. Bacterial colonies were counted subsequently after overnight incubation to obtain an estimation of the viable cells on each surface.

#### 2.10.3. Antibacterial Property of SA at Different pH

The growth curves of *S. aureus* were monitored in medium Tryptic Soy Broth (TSB) with 0.25% glucose, containing 500, 250 and 100 µg mL$^{-1}$ SA at different pH values (6.5, 7.4, and 8.5) using a plate reader (BioTek Synergy H1 Multimode Reader) for 24 h. Medium without bacterial inoculum was used as a negative control, and that with bacteria as a positive control.

### 2.11. Cell Culture

All cells were cultured at standard culture conditions of 37 °C, with 5% $CO_2$ and 95% humidity, and cells were counted using a CASY cell counter and analyzer (OMNI Life Science Innovatis).

#### 2.11.1. THP-1 Macrophages

Macrophage-like cells were generated using a human monocytic leukemia cell line (THP-1, ECACC 88081201, UK). THP-1 cells were expanded in growth medium consisting of RPMI 1640 Medium (Sigma) supplemented with 10% FBS, 1% P/S and 1% L-glutamine ($2 \times 10^{-3}$ M Sigma) and differentiated into macrophage-like cells by supplementing the medium with $100 \times 10^{-9}$ M phorbol myristate acetate (PMA; Sigma) for 3 d. To stimulate a proinflammatory (M1-like) phenotype, macrophages were subjected to (M1 medium containing 100 ng mL$^{-1}$ LPS (Sigma) and 20 ng mL$^{-1}$ interferon-$\gamma$ (IFN- $\gamma$, Miltenyi Biotec, Switzerland)), while anti-inflammatory (M2-like) phenotype was stimulated by the addition of M2 medium containing 20 ng mL$^{-1}$ interleukin-4 (Miltenyi Biotec), as previously reported.[37] TripLE Express was used for trypsinization of THP-1 cells. THP-1 Macrophage-like cells were seeded at a density of 150 000 cells per well, on a glass coverslip with 15 mm diameter, resulting in a density of 85 000 cells cm$^{-2}$ for gene expression analysis. THP-1 cells were used between passage 6–18.

#### 2.11.2. Human Gingival Cells

Primary human gingival fibroblasts (HGFs, ScienCell, USA) isolated from human gingiva were cultivated in growth medium comprising Dulbeco's modified Eagle's medium (DMEM, 4.5 g L$^{-1}$ glucose, Sigma, Switzerland), supplemented with 10% heat inactivated fetal bovine serum (FBS, Sigma) and 1% penicillin-streptomycin (5 mg mL$^{-1}$) antibiotic–antimycotic cocktail (Sigma), and trypsin was used for trypsinization. For differentiation of these cells into the myofibroblast phenotype, this medium composition was modified to differentiating medium containing RPMI-1640 medium (Gibco) with 1% horse serum and transforming growth factor $\beta$ (TGF- $\beta$, 2 ng mL$^{-1}$), keeping the other components identical. After HGFs reached a confluency of 80–90% cells were first washed with RPMI-1640 without any supplements (to remove residual FBS) before incubating them in differentiation medium for 3 d. To assess the anti-inflammatory potential of the coating, salicylic acid ($0–4.5 \times 10^{-3}$ M) was also added during differentiation. HGFs were seeded at a density of 30 000 cells cm$^{-2}$ for gene expression analysis. Growth medium was replaced every 2–3 d, and cells were detached using trypsin/ethylenediaminetetracetic acid (EDTA) at 70–90% confluency and used till passage 20.

#### 2.11.3. Human Bone Progenitor Cells

Human bone progenitor cells were isolated from the trabecular bone pieces of patients undergoing hip replacement surgeries after informed consent, as described earlier (Ethics approval EKOS 22/193. Ethikkommission Ostschweiz).[38] $\alpha$MEM (Gibco, Switzerland) supplemented with 10% fetal calf serum (FCS; Lonza, Switzerland), 1% penicillin-streptomycin (Sigma) and 1 ng mL$^{-1}$ basic fibroblast growth factor (Sigma) was used as proliferation medium for expanding cells. Cells were subcultured at a density of 2000 cells cm$^{-2}$ and cells from passage 2 were used for experiments. Cells were seeded on Ti samples at a seeding density of 20 000 cells cm$^{-2}$ with proliferation medium, which was replaced by osteogenic medium till day 28 that contained $\alpha$MEM supplemented with 10% FCS, 1% penicillin–streptomycin, $50 \times 10^{-6}$ M ascorbic acid (Sigma), $2 \times 10^{-3}$ M $\beta$ glycerol phosphate, $10 \times 10^{-9}$ M 1,25-dihydroxy-vitamin D3 (Sigma), and $10 \times 10^{-9}$ M dexamethasone (Sigma) (Vitamin D3 and dexamethasone were added freshly each time the medium was changed).

### 2.12. Assessment of Mineralization Potential of Bone Cells on the Coating

Human bone progenitor cells were seeded on coated Ti substrates, fixed (Section 2.11) and stained for nuclei (dapi) and actin (phalloidin) and imaged using the CLSM. After 28 d of culture in osteogenic medium, the mineralization potential of cells on different coatings was assessed using the calcium assay kit (Abnova Corporation, USA) according to manufacturer's protocols. Cells were lysed using 1 M hydrochloric acid (HCl) to solubilize calcium. The Ca content was normalized with the DNA that was measured for the same samples using the Quant-iT PicoGreen dsDNA assay kit (Thermo Fischer) after lysing cells in a lysis buffer ($150 \times 10^{-3}$ M NaCl, 1% Triton X, $50 \times 10^{-3}$ M Tris HCl, pH 7.4).

### 2.13. Blood-Coating Interactions

Glass substrates (5 mm diameter) with different coatings were incubated with whole human blood to assess the impact of the SA coating on blood coagulation. The coatings were sterilized with UV light for 40 min and placed in custom-made Teflon holders with holes of 5 mm diameter and 1 mm depth, with notches for insertion of tweezers, to prevent scratching the surface. All surfaces were incubated with partially heparinized (0.5 IU mL$^{-1}$ heparin, Sigma) whole human blood that is obtained by phlebotomy from healthy donors between 18 and 55 years (ethical approval was obtained from the local ethics committee; EKSG, BASEC Nr PB_2016_00816). Phlebotomy was performed by a trained medical doctor and blood was used within 1 h after withdrawal. 1.4 mL

of blood was added to each Teflon holder, that contained 3 samples, and different conditions were housed in different Teflon molds. After incubation for a specific time duration on a shaker at 10 rpm, the samples were washed with PBS 3 times and were then prepared for further analysis.

### 2.14. Scanning Electron Microscopy

Scanning electron microscopy was used to assess blood coagulation on the coatings. The samples were fixed with Karnovsky solution (4% paraformaldehyde, 2.5% glutaraldehyde) for 1 h, followed by washing with 1× PBS twice. Dehydration was performed using an increasing gradient of ethanol (50%, 70%, 80%, for 30 min each, followed by 90% and 100% ethanol for 1 h each. The final dehydration step was performed by immersing the substrates in hexamethyldisilazane for 30 min, after which the samples were allowed to air-dry overnight. These substrates were then mounted on aluminum stubs using a carbon tape (Ted-Pella) and coated with a 10 nm layer of gold/palladium (ACE 600, Leica Microsystems, Switzerland), before imaging with an accelerating voltage of 2.0 kV and a current of 10 µA using a Hitachi S-4800 device.

### 2.15. Immunohistochemistry

Confocal laser scanning microscopy (CLSM) was performed using a Zeiss LSM 780 (Zeiss, Germany) microscope. For this, cells are fixed with 4% paraformaldehyde (4% PFA; $25 \times 10^{-3}$ M HEPES, $10 \times 10^{-3}$ M EDTA, $3 \times 10^{-3}$ M $MgCl_2$, $65 \times 10^{-3}$ M PIPES (piperazine-N,N′-bis(2-ethanesulfonic acid)) and then permeabilized with 0.1% Triton X (Sigma) for 30 min. Blocking was performed with 3% bovine serum albumin (BSA) and 5% goat serum in PBS for 1 h. α-smooth muscle actin (αSMA) conjugated to FITC (Sigma F3777, 1:800 dilution, ≈2 µg $mL^{-1}$ final concentration) and collagen I (Abcam ab34710, ≈2 ng $mL^{-1}$) were used as primary antibodies and incubated overnight. Secondary antibody (AlexaFluor 555 conjugated anti-rabbit secondary antibody) was added (1:500, ≈2.5 µg $mL^{-1}$) in PBS for 1 h. Phalloidin (Invitrogen A22284) was diluted 1:200 while DAPI (Sigma D 9542) was diluted 1:1000 times for DNA staining.

### 2.16. Assessment of Cell Proliferation on the Coating Surface

The metabolic activity of cells on the different layers of the coating was assessed using the presto blue viability assay (Invitrogen), which detects the mitochondrial activity of living cells using a resazurin based dye. Cells were incubated with 10% (v/v) Presto Blue reagent in growth medium and incubated for 2 h at 37 °C, 5% $CO_2$. Fluorescence was measured at a wavelength of 547 nm (excitation) and 582 nm (emission) using a Mithras plate reader (Berthold technologies). Presto blue working solution without cells was used as blank.

### 2.17. Gene Expression Analysis

For assessing the differentiation of HGFs into myofibroblasts, the expression levels of RNA coding for *αSMA*, collagen I and *SMAD3* were evaluated. To determine the effect of salicylic acid in medium on the differentiation process, SA ($3 \times 10^{-3}$ M) was added to cells during differentiation (1% horse serum with 2 ng $mL^{-1}$ TGF-*β*) and cells are harvested at day 2 and 4 (Figure S8A, Supporting Information). The anti-inflammatory efficacy of the coating was evaluated using HGFs, which were seeded on the coating (substrate = 15 mm diameter glass coverslips) with a seeding density of 30 000 cells $cm^{-2}$. The release of SA from the coating was the source of SA here, so SA is not added to the differentiation medium. Differentiation medium was added to cells at day 1 after seeding, and cells were harvested at day 4. Total cell RNA was isolated and purified using the RNeasy Micro Kit (Qiagen, Germany), according to manufacturer's protocol. The RNA concentration and its purity was measured using the Nanodrop ND-1000 Spectrophotometer (Thermo Scientific). 150–500 ng RNA was reverse transcribed to cDNA using the iScript cDNA synthesis kit (Bio-Rad, Switzerland). This was followed by 5 min priming at 25 °C, reverse transcription at 42 °C for 30 min, and inactivation at 85 °C for 5 min. After cooling down to 4 °C, the cDNA was diluted in RNAse free water to a final concentration of 1.5 ng $\mu L^{-1}$ and stored at – 80 °C until use. cDNA was amplified in a quantitative PCR reaction using iQ SYBR Green supermix (BioRad) using manufacturersprotocols (DNA denaturation and polymerase activation at 95 °C for 5 min followed by 40 cycles of denaturation at 95 °C for 10 sec and annealing at 60 °C for 30 sec). All primers were used at a final concentration of $10 \times 10^{-6}$ M and are listed in Table below (**Table 1**). Reactions were performed using the CFX Opus 384 RT-PCR System (Bio-Rad).

THP −1 monocytes were first differentiated to THP-1 macrophages (Section 2.8.2) after which they were seeded on the coating and harvested after 24 h. The polarization of THP-1 macrophages was assessed using mRNA expression of following genes: C-C chemokine receptor type 7 (*CD197*), C-X-C motif chemokine 10 (*CXCL10*) and Mannose receptor C type 1 (*CD206*). To normalize the mRNA expression, two reference housekeeping genes were used: glyceraldehyde-3-phosphate dehydrogenase (*GAPDH*) and ribosomal protein L13 (*RPL13a*). As less variation was obtained, *RPL13a* was used as a reference gene for HGFs while *GAPDH* was used for THP-1 genes.

The fold change of gene expression was calculated using CT comparative method, which is also referred as $2^{-(\Delta\Delta C_T)}$ method and it is represented in Equation 2.

$$\text{Fold change} = 2^{-(\Delta\Delta C_t)} = 2^{-((\text{Ct gene of interest} - \text{Ct reference gene})\text{sample} - (\text{Ct gene of interest} - \text{Ct reference gene})\text{reference})} \quad (2)$$

**Table 1.** Table with the genes used in this study and the primer sequences.

| Gene (Abbreviation) | Forward primer sequence 5′ → 3′ | Reverse primer sequence 5′ → 3′ |
|---|---|---|
| Alpha smooth muscle actin (*αSMA*) | TGAGAAGAGTTACGAGTTGCC | GATGCCAGCAGACTCCATCC |
| C-C chemokine receptor type 7 (*CD197*) | GTGGTTTTACCGCCCAGAGA | CACTGTGGTGTTGTCTCCGA |
| Collagen I (*Col1A1*) | GAAGGGACACAGAGGTTTCAG | AGCTCCATTTTCACCAGGG |
| C-X-C motif chemokine 10 (*CXCL10*) | CAGTCTCAGCACCATGAATCAA | CAGTTCTAGAGAGAGGTACTCCTTG |
| Glyceraldehyde-3-phosphate dehydrogenase (*GAPDH*) | AGTCAGCCGCATCTTCTTTT | CCAATACGACCAAATCCGTTG |
| Mannose receptor C type 1 (*CD206*) | GCTACCCCTGCTCCTGGTTT | CGCAGCGCTTGTGATCTTCA |
| Ribosomal protein L13 (*RPL13a*) | AAGTACCAGGCAGTGACAG | CCTGTTTCCGTAGCCTCATG |
| *SMAD3* | CATCGAGCCCCAGAGCAATA | GTGGTTCATCTGGTGGTCACT |

### 2.18. Statistics

Each experiment was repeated at least 3 times in the form of 3 independent experiments containing a minimum of 3 samples per condition per time point, unless otherwise mentioned. Statistical significance was determined by Anova followed by a post-hoc Tukey test where normal distribution as determined by Levene's test was obeyed and with a Welch test followed by a Games-Howell post-hoc test where normal distribution was not obeyed. Statistical significance with the reference sample is represented by $p$ value, where *, **, *** corresponding to $p < 0.05$, 0.01 and 0.001, respectively.

## 3. Results and Discussion

### 3.1. Coating Strategy

The coating of titanium (Ti) implant surfaces with an organic polymer is challenging due to problems associated with interfacial adhesion that lead to non conformal and poor coating properties. As shown in Figure 1, glass or Ti surfaces are coated with Pda which is formed from dopamine upon oxidation (Step 1). While the exact polymerization mechanism of Pda formation is still debated, it is widely believed to be formed by the oxidation of dopamine, where covalent and noncovalent linkages contribute to its ability to adhere to different surfaces.[39] Pda increases the hydrophilicity of the Ti or glass substrate. The melt condensation technique is utilized to prepare prepolymers of the diacid and glycerol in the molar ratio 1:1, reported to result in the highest molecular weight. The prepolymer composed of the SA based diacid and glycerol has free hydroxyl as well as carboxylic groups, and is hence expected to react with the amino functionalities of the Pda layer to enable amide bond formation.[40]

In this study, two different approaches are pursued to investigate the binding properties of the Pda to the SA ester. In the first approach, we harness the unreacted amine and hydroxyl functional groups on the Pda surface to bind to free carboxylic groups on the SA ester. In the second approach, we introduce carboxylic groups to the Pda surface by conjugating SA based diacid through amine bonds (Figure S1, Supporting Information). The main idea is to not only increase the loading of SA in the coating but also to enable the linkage of the ester through the carboxylic groups on the diacid. Since the second synthesis approach involving the polydopamine layer decorated with the diacid (Pda + diacid) and with spin coated ester (Pda + diacid + SA ester) showed results that are largely similar to the first approach, the results are included in Figures S1–S6 and S9–S11 and Note S1, (Supporting Information). To enable the assessment of each layer of the coating that is sequentially added, we analyze the following groups: i) substrate without coating (Glass or Ti as control), ii) Pda coated substrate (Pda), iii) substrate coated with Pda, which is sequentially spin-coated with a layer of SA containing polyester (Pda + SA ester). The different steps used to prepare the coatings are described in Figure 1.

### 3.2. Surface Characterization of the Coating

#### *3.2.1. Confirmation of Sequential Coating Layers by Raman and Atomic Force Microscopy*

The sequential layers of the coating on polished Ti are assessed by Raman spectroscopy. The presence of Pda is confirmed from characteristic peaks for Pda at 1400 and 1570 $cm^{-1}$, respectively, corresponding to the stretching and deformation of catechol,[41–43] (Figure 2A). The broad shoulder around 3300 $cm^{-1}$ suggests that most of the —OH groups of the Pda coating are already coordinated with Ti.[44] This is supported by brightfield microscopy, which also showed the presence of (likely Pda) deposits on the surface (Figure 2B). The Pda-SA ester coated layer, on the other hand does not reveal the Pda peaks, but shows the presence of a phenyl ester peak at 1729 $cm^{-1}$ corresponding to the C═O of an aliphatic ester. In addition, the ester also displays a peak at 1638 $cm^{-1}$ assigned to the vibration of the aromatic C═O of SA. This peak is sharp in the SA ester, where H bonding is limited due to esterification.[33] Other peaks such as those at 1582 $cm^{-1}$ (small peak) and 1462 $cm^{-1}$ (large peak) corresponding to the C═C stretching of the benzene ring and at 1022 $cm^{-1}$ and 812 $cm^{-1}$ that are assigned to the C—C in plane bending also reaffirm the presence of the ester in Pda + SA ester.[45] Overall, the Raman spectra confirm that the Pda surface layer is covered by the sequential layer of the SA ester. The presence of SA ester on Pda + SA ester coating is established by the additional peaks observed in the Raman spectrum (Figure 2A). Moreover, we also observe that the SA ester peak disappears when the irradiation time of the Raman spectrometer laser is increased, (due to the removal of the ester layer) and reveals the Pda peaks from the underlying Pda layer. Finally, Raman mapping is used to monitor the homogeneity of the coating (Figure 2B). While it is common to observe some differences in the homogeneity,[45] our results

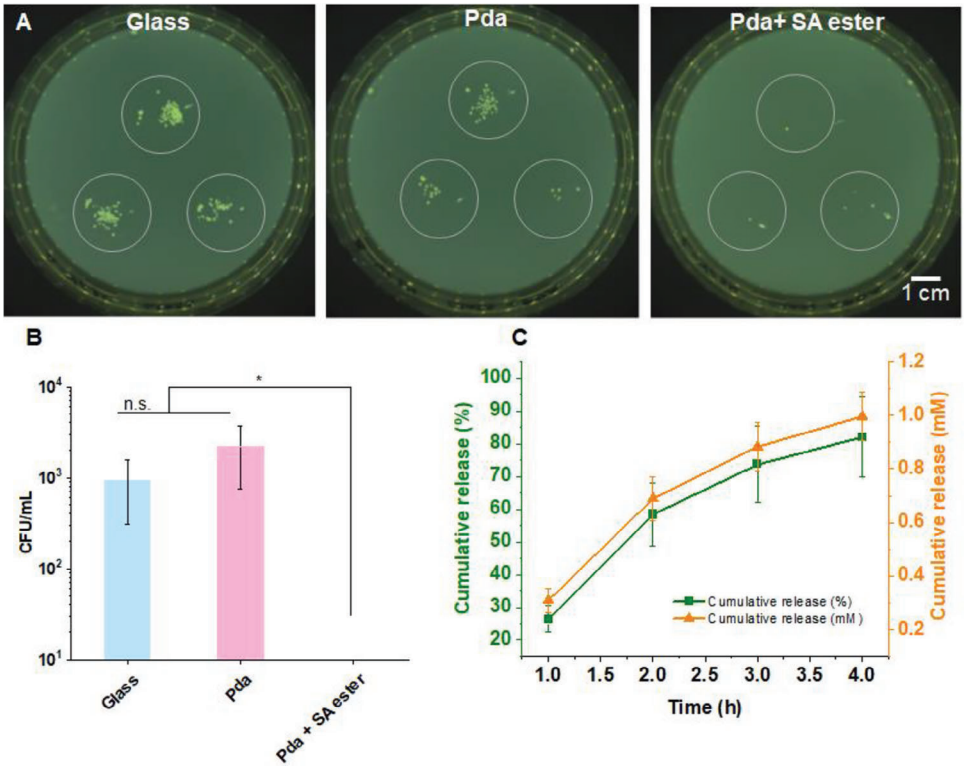


**Figure 3.** Evaluation of the antibacterial property of the coatings using *S. aureus*. A) Bacterial growth after incubation with different surfaces, analyzed using a touch assay. B) Quantitative analysis of the viable bacteria after incubation with different surfaces. C) Cumulative release of SA from Pda+SA ester coating as % of the total SA content as well as the calculated cumulative SA concentration over 4 h, the incubation duration for the touch assay. * represents statistical significance at $p < 0.5$.

show complete coverage of the substrate by Pda, with some inhomogeneities at the molecular level (Figure 2B). This is confirmed by the catechol stretch and deformation of Pda (1338–1638 $cm^{-1}$) map, as well as by the C=O (1715–1745 $cm^{-1}$) of SA in Pda+SA ester (Figure 2). This is direct evidence for the presence of two layers of the coating- the Pda layer and the spin coated SA ester covering the Pda layer. Figure S2 and Note S1 (Supporting Information) compare the coating with diacid.

AFM imaging of a scratch on the coating corroborated the observations from confocal Raman spectroscopy and confirmed the presence of sequential layers. The average thickness of the coating and the contribution of each layer is shown in Figure 2, as measured from the height sensor channel of the AFM (Figure 2C–E). The Pda layer contributes to a thickness of approximately 6 nm, while the spin coated layer is approximately 300 nm. X-ray photoelectron spectroscopy (XPS) is used to ascertain the surface chemical characterization of the coating. Pda and Pda + SA ester show 75.0 and 87.6 at% C and 20.4 and 12.01 at% O, respectively. The spectrum of the Pda coated substrate revealed the presence of nitrogen (N1s, 400 eV, Figure 2F), which is in accordance with the chemical composition of Pda (Figure 1). Furthermore, a N/C ratio of 0.061 is found for Pda, which is much lower than the theoretical value of 0.125, possibly due to the degradation of the surface during the measurement. On the coating with the SA ester, the nitrogen peak is absent confirming the presence of the SA ester on the surface (Figure 2F). The presence of diacid is confirmed by measuring the surface zeta potential (via streaming potential, Figure S3 and Note S2, Supporting Information).

The presence of the coating is further confirmed via water contact angle measurements (Figure S4, Supporting Information). The pristine polished Ti displays a contact angle of 62 ± 5°, whereas the presence of a Pda coated surface leads to a contact angle of 53.4 ± 3° due to the more hydrophilic nature of Pda.[40] The spin coated SA ester (Pda + SA ester) shows a contact angle of 33.4 ± 5.6°, which could be due to the presence of some unreacted and free hydroxyl and carboxylic groups that contribute to the hydrophilicity, in spite of the presence of hydrophobic SA.[46] Overall, the chemical characterization of the sequential coating layers confirmed the presence of SA ester on the coating surface.

### 3.3. Antibacterial Property of the Coating

*S. aureus* is known to be a major contributing factor in peri-implantitis development as it exhibits a very high affinity to titanium,[6] and is hence used as a model bacterial strain to investigate the anti-bacterial efficacy of the fabricated coatings.

SA is a well-known anti-bacterial agent with a minimum inhibitory concentration of 250–500 μg $mL^{-1}$ (1.81–3.6 × 10 × $10^{-3}$ M) against *S. aureus*.[47] The SA containing surface of Pda + SA ester fabricated in this work inhibited the growth of *S. aureus* in a touch assay[48] (**Figure 3**A). Quantitative analysis of the antibacterial activity revealed that Pda+ SA ester coating completely

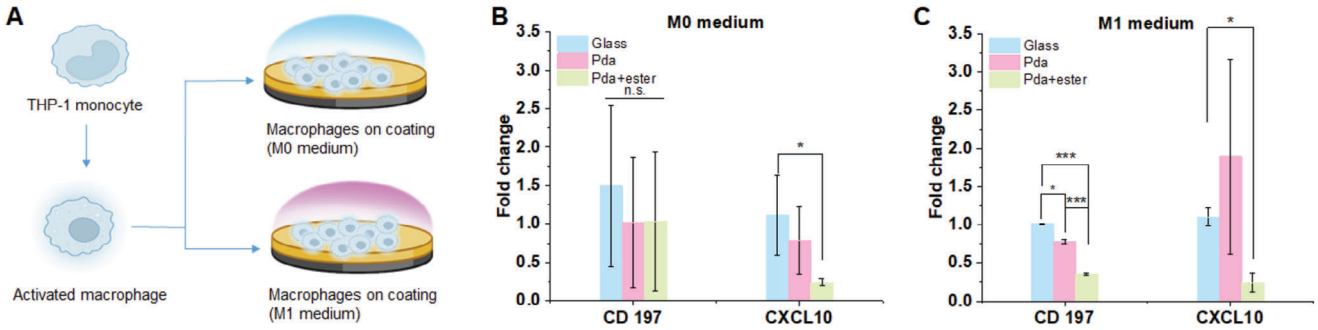


**Figure 4.** A) Schematic showing the differentiation of THP-1 monocytes into macrophage-like cells that are incubated on the surface of coatings in the presence of M0 medium to mimic a healthy condition or M1 medium (supplemented with lipopolysaccharides (LPS) and interferon $\gamma$ (IFN-$\gamma$)) to mimic an inflamed condition. Gene expression of *CD197* and *CXCL10* in M0 medium, B) $N = 2$, $n = 2$ and M1 medium, C) $N = 3$, $n = 2$, both with *GAPDH* used as a reference gene and fold change compared to uncoated glass surface after 24 h of cultivation on the surface of the coatings. *, **, *** represent statistical significance at $p > 0.5$, 0.1 and 0.001, respectively. Image in A created with BioRender.com.

eliminated bacterial growth, whereas the control samples of uncoated glass and Pda + glass led to approximately 941 ± 634 and 2222 ± 1464 CFU mL$^{-1}$, respectively (Figure 3B).

The coating is expected to undergo hydrolysis, which leads to release of SA, along with glycerol and sebacic acid. To interpret the dose correlation of our data, we measured the release of SA from Pda + SA ester in PBS via UV–vis spectroscopy and determined the cumulative release (%) as well as the concentration (Figure 3C and Figure S5D and Note S3, Supporting Information). Considering a cumulative release, we estimate a concentration of $0.93 \times 10^{-3}$ M SA in the bacterial inoculum at the end of the 4 h period (Figure 3C). Thus, we observe that even a low loading of (≈8 µg) of SA per coated sample (coating thickness approximately 300 nm, sample diameter 15 mm) still has a positive influence on bacterial reduction.

Since the pH in the vicinity of a failed implant is more acidic compared to the environment of a healthy tooth,[49] we further evaluated the bacteriostatic potential of SA in solution at different pH (6.5, 7.4 and 8.5) at different concentrations of 100, 250, and 500 µg mL$^{-1}$ (Figure S5F–H, Supporting Information). These results show that at a concentration of 100 µg mL$^{-1}$ SA ($0.72 \times 10^{-3}$ M) results in a CFU mL$^{-1}$ decrease of 31.9%, 22.6%, and 16.5% at pH 6.5, 7.4 and 8.5, respectively, when compared with the positive control (without SA). Thus the higher bacteriostatic activity of SA at low pH, which is associated with failed implants, becomes advantageous.

### 3.4. Immunomodulation of Macrophages via SA Containing Coating

Since macrophages are important mediators of an immune response and perform various functions involving host defense and tissue healing after implantation, we assess macrophage polarization of cells grown on the coating. Conventionally, the two extremes are the proinflammatory M1-like subtype and the anti-inflammatory M2-like subtype involved in tissue healing.[50] We do not observe a significant difference in the viability of THP-1 monocytes that maturated into THP-1 macrophages on the surface of differently coated glass substrates at day 1 in M0 (basal medium) as well as in M1 (proinflammatory medium) (Figure S6A, Supporting Information). The immunomodulatory potential of the SA containing coating is assessed by gene expression analysis of M1 and M2 representing marker genes coding cytokines. The expression of M1-like markers *CD197* and *CXCL10* in cells grown on Pda + SA ester shows a significant reduction in expression (65% for *CD197* in M1 medium and ca. 75% for *CXCL 10* in M0 and M1 medium) compared to the expression in cells on the uncoated substrate in the same medium (**Figure 4**). A similar trend is observed in the Pda+ diacid + ester coating, with *CD197* showing a reduction of c.a. 55% in M1 medium as compared to the glass control (Figure S6B,C, Supporting Information). In addition, we also evaluate an M2 polarization marker gene *CD206*, where we do not observe significant increase as compared to glass in both, M0 and M1 medium (Figure S6D, Supporting Information). These observations confirm that the SA containing coating facilitates a micro-environment for cells that results in reduced expression of M1-like or proinflammatory markers (*CD197* and *CXCL10*). Aspirin has been shown to inhibit LPS-induced macrophage activation, here we demonstrate the effect of deacetylated aspirin (SA) release that results in decreased levels of M1 markers.[51]

### 3.5. Effect of SA on Fibroblast and Osteoblast Differentiation

We aim to design a coating that does not jeopardize the natural healing ability of the tissue surrounding an implant due to complete elimination of the myofibroblast phenotype. Hence, we first investigate the effect of SA dissolved in medium on the viability of human gingival fibroblasts, and conclude that $3 \times 10^{-3}$ M of SA represents the maximal concentration that can be used without adversely affecting viability (Figure S7 and Note S4, Supporting Information). Immunohistochemical staining and imaging using confocal microscopy demonstrate a qualitative decrease in *αSMA* with increasing concentration of SA (Figure S8, Supporting Information). To verify the influence of SA added to cell culture medium during differentiation into myofibroblasts, we evaluated the gene expression of *αSMA*, collagen I (*Col1A1*) and the tumor suppressor factor Suppressor of Mothers against decapentaplegic homolog (*SMAD3*) (**Figure 5**B–D). Upon treating cells with TGF-$\beta$ in the absence of SA (positive control), an

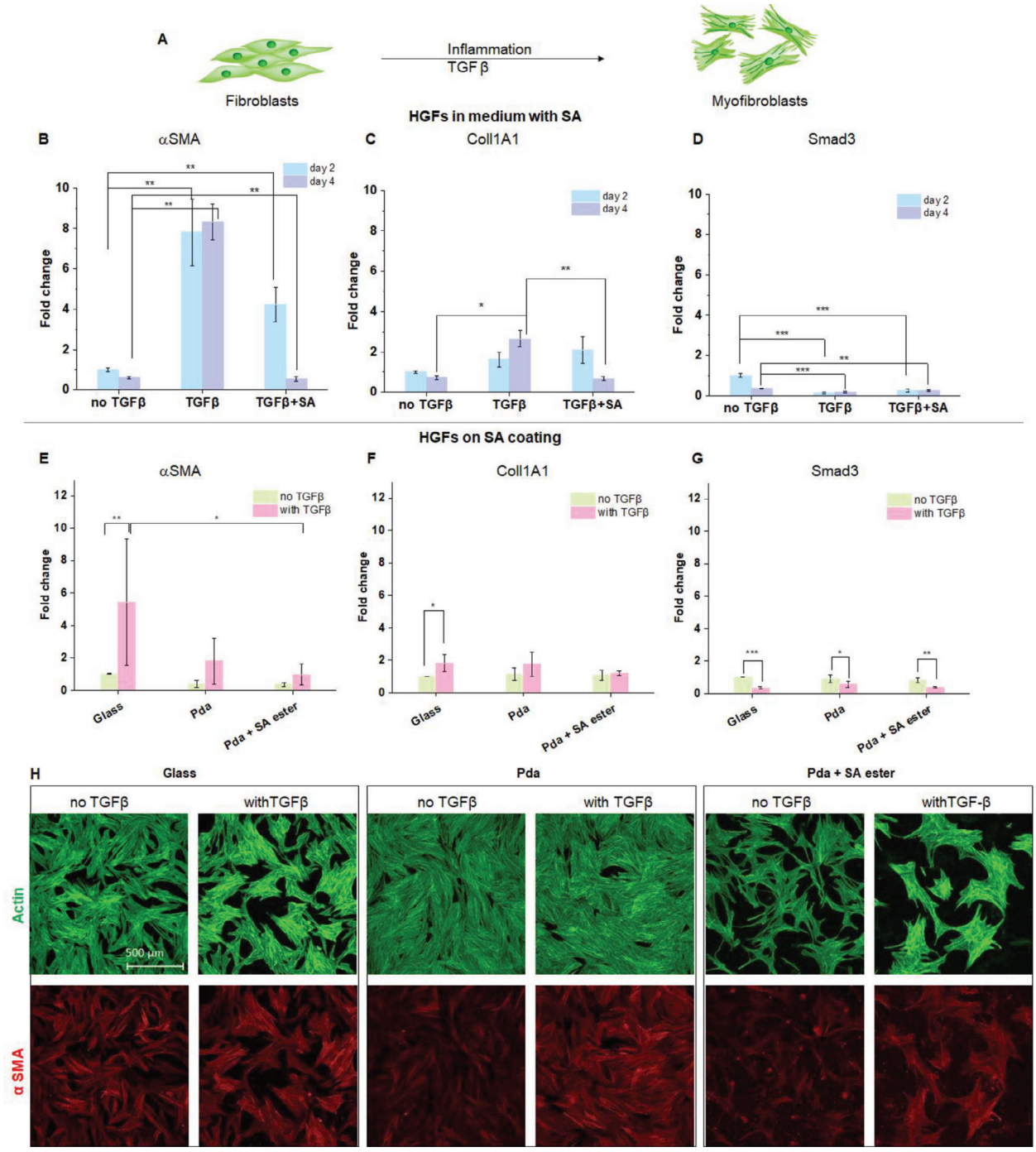


**Figure 5.** A) A schematic showing the concept of evaluation of the anti-inflammatory potential of SA by assessment of the transformation of human gingival fibroblasts (HGFs) to myofibroblasts. B–D) Gene expression assessment by PCR for HGFs without TGF-$\beta$ and with TGF-$\beta$ when $3 \times 10^{-3}$ M SA is added to the medium and E–G) when HGFs are cultivated on glass, Pda and Pda + SA ester for B,E) *αSMA* C,F) *Col1A1*, D,G) *SMAD3* ($N = 3$, $n = 2$). Confocal laser scanning microscopy images of HGFs grown in starve medium for 3 d without TGF-$\beta$ and with TGF-$\beta$ stained for actin (green), αSMA (red). Scale bar = 500 μm. *, **, *** represent statistical significance at $p < 0.05$, 0.01 and 0.001, respectively.

increase in the mRNA level of *αSMA* and *Col1A1* by 7.8 ±1.6 and 1.6 ± 0.3-fold on day 2 and by 8.3 ± 0.8 and 2.6 ± 0.4 fold on day 4, respectively, is observed when compared to the basal production of these genes (Figure 5A). This is expected, since differentiation of HGFs in the presence of TGF-$\beta$ promotes myofibroblast differentiation, which is characterized by upregulation of the aforementioned genes. The addition of $3 \times 10^{-3}$ M of SA to the medium does not affect myofibroblast differentiation (4.2 ± 0.8 fold change compared to 7.8 ± 1.6 in the presence of TGF-$\beta$ without SA for *αSMA and* 2.1 ± 0.6 for *Col 1A1* in the presence of

TGF-$\beta$ and $3 \times 10^{-3}$ M SA and 1.6 ± 0.3 only with TGF-$\beta$ without SA) for day 2. On day 4, however, SA addition significantly lowers the expression of *αSMA and Col 1A1* to 0.55 ± 0.1 and 0.68 ± 0.1, respectively. Taken together, these findings suggest that the addition of SA to HGFs during myofibroblast differentiation allows an initial peak of myofibroblast expression at day 2, which subsides by day 4 and shows only mild down-regulation of typical myofibroblast-associated genes. We believe that such a pattern of myofibroblast phenotype which is present in the early stages of wound healing and then is suppressed would be very favorable after implantation, since it is similar to normal wound healing with fast resolution of inflammation in gingival fibroblasts.[52]

Based on the above results obtained for cells in the presence of SA in medium, we hypothesize that the release of SA from the coating can initially allow myofibroblast activity and reduce it at later timepoints (day 4). Hence, we coat glass substrates with Pda or with Pda + SA ester and assess the effect of the SA released from the coating on *αSMA*, *Col1A1* and *SMAD3* in healthy (no TGF-$\beta$) and inflamed/wound mimicking environment (with TGF-$\beta$) (Figure 5). Upregulation of *αSMA* (5.4 ± 3.9 fold) and *Col1A1* (1.8 ± 0.5 fold) on the glass control without any coating upon addition of TGF-$\beta$ at day 4 confirms myofibroblast formation. In an inflammation mimicking scenario (with TGF-$\beta$), the coating results in statistically significant lowering of *αSMA* expression and reduces the levels from 5.4 ± 3.9 (glass) to 0.9 ± 0.6. We assess the expression of *SMAD 3*, which is not affected by the coating, and displays reduced expression on the glass control, Pda and Pda + SA ester in the presence of TGF-$\beta$ (Figure 5D). Staining of the expressed proteins by immunocytochemistry techniques also shows the same trend for *αSMA* and *Col1A1*, with only a mild decrease on day 4 (Figure 5F). The expression of *Col1A1* also shows a slight down regulation in response to the SA released by the ester coating, although this is not statistically significant. These observations are in line with the trend that we observed with SA added to medium. In the context of gingival myofibroblasts, scar formation is less likely compared to other parts such as skin, and is also thought to be due to precise control of cellular microenvironment of gingival myofibroblasts compared to dermal fibroblasts.[53] The coating supports healing in way that is similar to natural scarless healing and is in line with the general trend shown by gingival fibroblasts where the myofibroblast phenotype is quickly resolved.

Non-steroidal anti- inflammatory drugs (NSAIDS) are known to negatively influence bone healing due to their effects on suppression of cyclooxygenase, which is required for prostaglandin synthesis, which are in turn required for fracture healing.[54,55] Due to the local release of SA from the coating, we investigate how this could potentially impact implant osseointegration by culturing human bone progenitor cells on coated Ti substrates. After one day of culture, cell morphology and spreading do not show differences between pristine Ti and the different coating layers (Figure S10A–E, Supporting Information). After 28 d in osteogenic medium, we assess the calcium (Ca) production in these differentiated cells to evaluate the mineralization potential (Figure S10F, Supporting Information). No significant differences are observed between any of the coatings and pristine Ti, confirming that the coatings do not negatively influence mineralization. SA is reported to locally inhibit bone loss and bone formation due to the effect on osteoclasts that leads to increased bone absorption and anabolic effect on osteoblasts at a concentration of 1.3 g $cm^{-3}$.[56,57] Theoretical estimates suggest that the concentration of SA is approximately 0.408 mg $cm^{-3}$ in our experiments, which could be a reason for why we do not observe a negative effect on bone mineralization. Another limitation of this experiment is that it was performed only with three biological replicates and one experimental replicate.

### 3.6. SA in Coating Modulates Blood-Coating Interactions

Surface chemistry is known to have an influence on protein adsorption. As blood is the first tissue that would potentially contact the coated implant surface, we incubate coated glass substrates with fresh, partially heparinized blood and assess fibrin clot formation and platelet morphology after 30 min and 60 min of incubation. While the control (glass without coating) shows progressive clot formation with a clearly visible fibrin network forming over time, the Pda coating alone shows fibrinogen adsorption, but only limited fibrin network formation at the latter timepoint (**Figure 6**). On the Pda + SA ester coating, fibrinogen adsorption is not visible (at the chosen conditions for imaging) and also no fibrin network is formed.

Platelets are present in high numbers on the uncoated control and trigger fibrin clot formation (Figure 6B,C) as seen in the actin staining. Platelets are well spread on the Pda coating layer (Figure 4B) but do not adhere to the Pda + SA ester coating. Thus the SEM and immunofluorescence observations corroborate with each other. To rule out auto-fluorescence effects in immunostained cells, we also examine different coating layers without blood incubation with SEM and immunofluorescence as control, whereby we conclude that the observed effects can be attributed to the presence of SA (Figure S11C,D, Supporting Information) alone. Pda + diacid + SA ester triggers similar results as Pda + SA ester (Figure S11 and Note S5, Supporting Information). Due to the low $pK_{a1}$ (2.8) of SA, at physiological pH of 7.4, SA is expected to exist in the form of salicylate.[58] One potential reason for the anti-coagulation effect that we observe in the presence of SA could be the reduction in the concentration of thromboxane (produced by aggregating platelets) by salicylates.[26] In the context of dental implant, it is reported that keratinocytes, which are typically very sensitive toward Ti surface properties, attach in the presence of a low amount of fibrin network .[59] The absence of $\alpha_v\beta_3$ integrins on keratinocytes prevents them from attaching to fibrin/ fibrinogen rich surfaces, in fact fibrin and fibrinogen are anti-adhesive for keratinocytes.[9] Keratinocytes can attach on other proteins such as fibronectin (mediated by $\alpha_5\beta_1$ integrin[60]), on vitronectin (mediated by $\alpha_5\beta_5$ integrin[61]) and on collagen (mediated by $\alpha_2\beta_1$ integrin).[60] Since a keratinized mucosa barrier around implants is thought to be required to prevent bacterial invasion and plaque accumulation,[62] this feature of the coating that prevents fibrin clot formation on the implant surface is expected to better support the formation of a keratinized mucosa. After the release of SA from the coating, we expect that adhesion of other cells (such as fibroblasts), which are capable of adhering to fibrin coated surfaces is facilitated. After the release of SA from the coating, we expect that adhesion of other cells (such as fibroblasts), which are capable of adhering to fibrin coated surfaces is facilitated.[59]

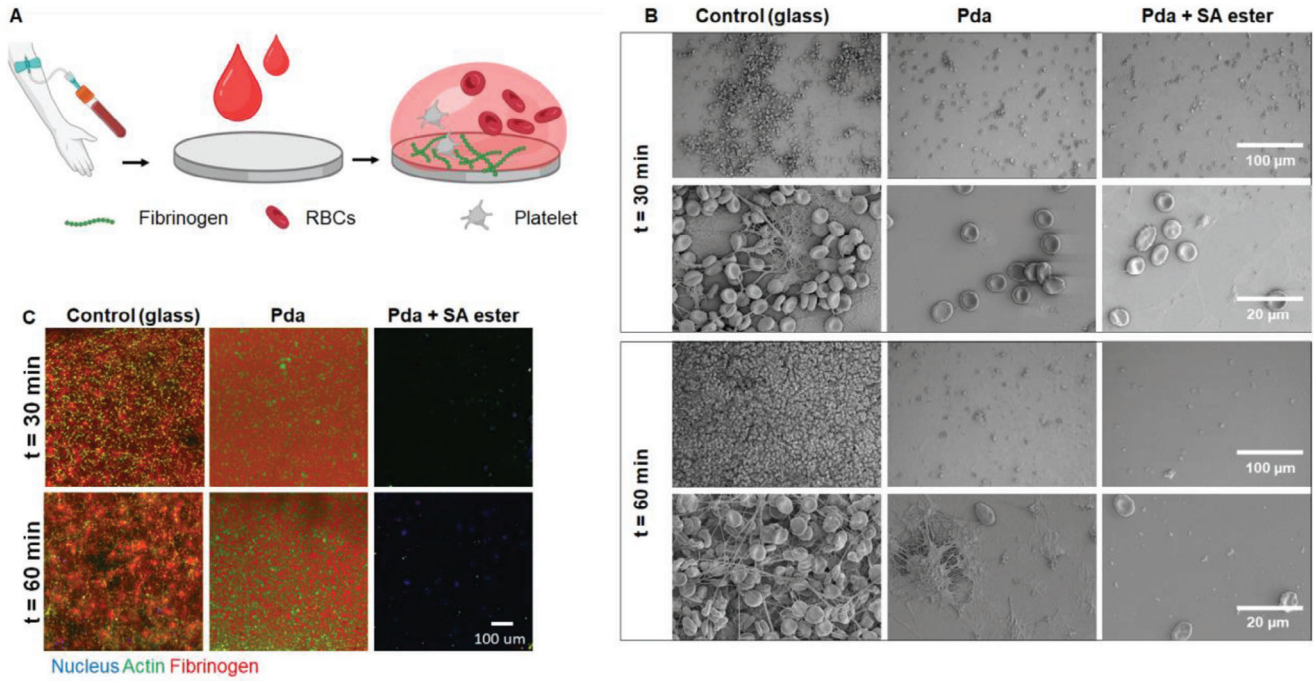


**Figure 6.** A) Schematic showing the steps involved in assessing the anti-coagulation activity of the coating. Different samples are incubated with blood. B) Scanning electron microscopy images of the substrate (glass) without any coating, which is used as control, Pda coated glass and Pda+ SA ester coated glass after 30 min (top two rows) and 60 min bottom two rows) showing the absence of platelets on the Pda+SA ester coated substrate. Scale bar = 100 µm in row 1 and 3, and 20 µm in row 2 and 4. C) Immunohistochemically stained blood cells incubated on uncoated glass, Pda and Pda+ SA ester coated glass showing nuclei that represent blood cells other than red blood cells (RBCs) and platelets, actin in green that represents RBCs and platelets and fibrinogen (red) obtained by confocal scanning microscopy. Image in A created with BioRender.com.

We conclude that the blood anticoagulation property of the coating is an indirect proof for the bioactivity of SA in the coating, and also its dosing which, in the early stages of implantation can potentially support keratinocyte attachment.

## 4. Conclusion

Here we test the hypothesis that local release of SA, a common non-steroidal anti-inflammatory drug for a few hours after implantation can be helpful to achieve anti-bacterial property and promote peri-implant healing. We show the anti-bacterial nature of the coating against *S. aureus* as well as the decreased production of pro-inflammatory markers such as *CD197* and *CXCL10 by* THP-1 derived macrophage-like cells on the coating surface. The coating also supports healing that is similar to natural scarless healing, as shown by the fast resolution of myofibroblast phenotype, and hence, does not pose the risk of fibrosis. Although NSAIDs are known to adversely affect bone formation, we show that the mineralization capacity of human bone progenitor cells is not affected. Due to the anti-coagulation property of SA, blood clot formation on the surface of the implant is reduced, which is a desirable attribute since it is known to aid keratinocyte attachment and promote the formation of a gingival seal. Further, tuning the dosage of SA from this coating by controlling coating thickness is a potential way to customize the dose response. The SA based coating designed is facile, easy to produce, is a cost-effective alternative to expensive peptides, and can be an effective approach in enhancing implant acceptance in dental implantology and beyond.

## Supporting Information

Supporting Information is available from the Wiley Online Library or from the author.

## Acknowledgements

Support from Dr. Matthias Wiesli for blood collection is greatly appreciated. The authors are also grateful to Stefanie Guimond for support with scanning electron microscopy, Stefanie Altenried for support with bacterial experiments, Thomas Ramsauer for evaluation of salicylic acid release through the coating, and Rico Muff for support with Raman microscopy. The authors are grateful to Raphael Wagner from Straumann AG for providing Ti samples. Y.C. acknowledges financial support from Marie Skłodowska-Curie grant agreement 754364, which is funded by the European Union's Horizon 2020 research and innovation. N.K. acknowledges financial support from the Swiss National Science Foundation, grant number 200021_192225.

## Conflict of Interest

The authors declare no conflict of interest.

## Author Contributions

Y.C.: Conceptualization and designing the coating for release of salicylic acid, methodology, validation, data curation, data analysis,

writing—original draft, visualization, supervision, project administration, funding acquisition. M.V.: Validation and investigation of coating synthesis, methodology, data curation, data analysis. B.K.: Validation and investigation of SA release on NHDFs, data curation, data analysis. Y.E.G.: Validation and investigation of immunomodulatory potential of the coating, data curation, data analysis. F.Z.: Validation and investigation of anti-bacterial potential of the coating, writing- review and editing. J.S.: Validation and investigation of the coating surface by XPS, support for streaming potential measurements, data analysis, writing- review and editing. N.K.: Validation and investigation of the coating thickness by AFM, data analysis, writing-review and editing. Q.R.: Methodology for the antibacterial potential of the coating, supervision, writing-review and editing. M.R.: Conceptualization, methodology for anti-thrombotic potential, gene expression analysis, anti-inflammatory potential of the coating, supervision, funding acquisition, writing-review and editing. K.M.-W.: Conceptualization of the study, supervision, project management, funding acquisition, writing-review and editing. All authors have read the final version of the manuscript and confirm their permission for publication.

## Data Availability Statement

The data that support the findings of this study are available in the supplementary material of this article.

## Keywords

antibacterial coating, bioactive coating, blood response, immunomodulatory coating, local drug release

Received: September 6, 2023
Revised: November 23, 2023
Published online:

[1] M. A. Saghiri, P. Freag, A. Fakhrzadeh, A. M. Saghiri, J. Eid, *Bull. Natl. Res. Cent.* **2021**, *45*, 7.
[2] N. Thiebot, A. Hamdani, F. Blanchet, M. Dame, S. Tawfik, E. Mbapou, A. A. Kaddouh, A. Alantar, *J. Oral Med. Oral Surg.* **2022**, *28*, 19.
[3] I. Dib-Zaitum, Y. Guadilla-González, J. Flores-Fraile, J. Dib-Zakkour, L. Benito-Garzón, J. Montero, *Materials* **2022**, *15*, 4422.
[4] G. Charalampakis, Å. Leonhardt, P. Rabe, G. Dahlén, *Clin. Oral Implants Res.* **2012**, *23*, 1045.
[5] K. Kordbacheh Changi, J. Finkelstein, P. N. Papapanou, *Clin. Oral Implants Res.* **2019**, *30*, 306.
[6] R. Smeets, A. Henningsen, O. Jung, M. Heiland, C. Hammächer, J. M. Stein, *Head Face Med.* **2014**, *10*, 34.
[7] N. Esfahanizadeh, S. Motalebi, N. Daneshparvar, N. Akhoundi, S. Bonakdar, *Lasers Med. Sci.* **2016**, *31*, 863.
[8] D. Graves, Y. Cao, P. Coelho, L. Witek, K. Uhrich, in *Emerging Therapies in Periodontics*, S. E. Sahingur, Springer International Publishing, Cham, Switzerland **2020**, pp. 43–53.
[9] M. Kubo, L. Van De Water, L. C. Plantefaber, M. W. Mosesson, M. Simon, M. G. Tonnesen, L. Taichman, R. A. F. Clark, *J. Invest. Dermatol.* **2001**, *117*, 1369.
[10] N. A. Valente, S. Andreana, *J. Periodontal Implant Sci.* **2016**, *46*, 136.
[11] G. Salehi, A. Behnamghader, M. Mozafari, in *Handbook of Biomaterials Biocompatibility*, (Ed: M. Mozafari), Elsevier, Amsterdam **2020**, pp. 453–471.
[12] S. Kligman, Z. Ren, C.-H. Chung, M. A. Perillo, Y.-C. Chang, H. Koo, Z. Zheng, C. Li, *J. Clin. Med.* **2021**, *10*, 1641.
[13] B. Hinz, *Curr. Res. Transl. Med.* **2016**, *64*, 171.
[14] H. Li, C. Guo, Y. Zhou, H. Sun, R. Hong, D. W. Hamilton, *Materials* **2021**, *14*, 6447.
[15] D. J. Gordon, D. D. Bhagawati, C. J. Pendegrass, C. A. Middleton, G. W. Blunn, *J. Biomed. Mater. Res., Part A* **2010**, *94*, 586.
[16] G. Schmidmaier, M. Lucke, B. Wildemann, N. P. Haas, M. Raschke, *Injury* **2006**, *37*, S105.
[17] J. A. Shibli, D. S. Ferrari, R. S. Siroma, L. C. D. Figueiredo, M. D. Faveri, M. Feres, *Braz. Oral Res.* **2019**, *33*, 1.
[18] K. V. Holmberg, M. Abdolhosseini, Y. Li, X. Chen, S.-U. Gorr, C. Aparicio, *Acta Biomater.* **2013**, *9*, 8224.
[19] M. Gabriel, K. Nazmi, E. C. Veerman, A. V. Nieuw Amerongen, A. Zentner, *Bioconjugate Chem.* **2006**, *17*, 548.
[20] S. K. Boda, C. Aparicio, *Biomater. Sci.* **2022**, *10*, 665.
[21] N. G. Fischer, D. G. Moussa, E. P. Skoe, D. A. De Jong, C. Aparicio, *ACS Biomater. Sci. Eng.* **2020**, *6*, 4929.
[22] M. Herrmann, *J. Clin. Invest.* **2003**, *112*, 149.
[23] Y. Chandorkar, N. Bhaskar, G. Madras, B. Basu, *Biomacromolecules* **2015**, *16*, 636.
[24] E. Stone, *Philos. Trans. R. Soc. London* **1763**, *53*, 195.
[25] R. Amann, B. A. Peskar, *Eur. J. Pharmacol.* **2002**, *447*, 1.
[26] G. A. Higgs, J. A. Salmon, B. Henderson, J. R. Vane, *Proc. Natl. Acad. Sci. USA* **1987**, *84*, 1417.
[27] C. J. Needs, P. M. Brooks, *Clin. Pharmacokinet.* **1985**, *10*, 164.
[28] M. A. Ali, J. I. Routh, *Clin. Chem.* **1969**, *15*, 1027.
[29] R. C. Schmeltzer, K. E. Schmalenberg, K. E. Uhrich, *Biomacromolecules* **2005**, *6*, 359.
[30] Y. Wang, G. A. Ameer, B. J. Sheppard, R. Langer, *Nat. Biotechnol.* **2002**, *20*, 602.
[31] G. Mingrone, L. Castagneto-Gissey, K. Macé, *Br. J. Clin. Pharmacol.* **2013**, *75*, 671.
[32] J. Tamada, R. Langer, *J. Biomater. Sci., Polym. Ed.* **1992**, *3*, 315.
[33] Y. Chandorkar, R. K. Bhagat, G. Madras, B. Basu, *Biomacromolecules* **2014**, *15*, 863.
[34] A. R. Fersht, W. P. Jencks, *J. Am. Chem. Soc.* **1970**, *92*, 5432.
[35] T. Amir, G. Weber, C. Beard, J. Bomyea, *Bone* **2008**, *23*, 1.
[36] H. Lee, S. M. Dellatore, W. M. Miller, P. B. Messersmith, *J. Chem. Inf. Model.* **2007**, *218*, 426.
[37] V. Malheiro, Y. Elbs-Glatz, M. Obarzanek-Fojt, K. Maniura-Weber, A. Bruinink, *Sci. Rep.* **2017**, *7*, 42495.
[38] B. S. Kopf, A. Schipanski, M. Rottmar, S. Berner, K. Maniura-Weber, *Acta Biomater.* **2015**, *19*, 180.
[39] J. H. Ryu, P. B. Messersmith, H. Lee, *ACS Appl. Mater. Interfaces* **2018**, *10*, 7523.
[40] W. Sheng, B. Li, X. Wang, B. Dai, B. Yu, X. Jia, F. Zhou, *Chem. Sci.* **2015**, *6*, 2068.
[41] L. Jiang, G. Jin, J. Kang, L. Yu, W. Yoon, M. Lim, I. Par K, M. Lee, D. Jin, *J. Wuhan Univ. Technol., Mater. Sci. Ed.* **2014**, *29*, 197.
[42] J. Ryu, S. H. Ku, H. Lee, C. B. Park, *Adv. Funct. Mater.* **2010**, *20*, 2132.
[43] S. H. Ku, J. Ryu, S. K. Hong, H. Lee, C. B. Park, *Biomaterials* **2010**, *31*, 2535.
[44] B. Fei, B. Qian, Z. Yang, R. Wang, W. C. Liu, C. L. Mak, J. H. Xin, *Carbon* **2008**, *46*, 1795.
[45] H. Eksi-Kocak, S. Ilbasmis Tamer, S. Yilmaz, M. Eryilmaz, I. H. Boyaci, U. Tamer, *Asian J. Pharm. Sci.* **2018**, *13*, 155.
[46] G. S. Denisov, N. S. Golubev, V. M. Schreiber, S. S. Shajakhmedov, A. V. Shurukhina, *J. Mol. Struct.* **1997**, *436–437*, 153.
[47] A. Adamczak, M. Ozarowski, T. M. Karpinski, *J. Clin. Med.* **2019**, *9*, 109.
[48] M. Zabara, Q. Ren, H. Amenitsch, S. Salentinig, *ACS Appl. Bio Mater.* **2021**, *4*, 5295.
[49] D. Karpavicius, M. Stasikelyte, N. Baseviciene, U. Sakalauskaite, S. Ratkute, D. Razukevicius, *Clin. Exp. Dent. Res.* **2019**, *5*, 236.
[50] M. Jaguin, N. Houlbert, O. Fardel, V. Lecureur, *Cell. Immunol.* **2013**, *281*, 51.
[51] Y. Liu, S. Fang, X. Li, J. Feng, J. Du, L. Guo, Y. Su, J. Zhou, G. Ding, Y. Bai, S. Wang, H. Wang, Y. Liu, *Sci. Rep.* **2017**, *7*, 11549.

[52] W. Mah, G. Jiang, D. Olver, G. Cheung, B. Kim, H. Larjava, L. Häkkinen, *PLoS One* **2014**, *9*, e90715.
[53] K. Mak, A. Manji, C. Gallant-Behm, C. Wiebe, D. A. Hart, H. Larjava, L. Häkkinen, *J. Dermatol. Sci.* **2009**, *56*, 168.
[54] J. Cottrell, J. P. O'connor, *Pharmaceuticals* **2010**, *3*, 1668.
[55] A. M. Simon, J. P. O'connor, *J Bone Jt. Surg. Am.* **2007**, *89*, 500.
[56] R. D. Harten, D. J. Svach, R. Schmeltzer, K. E. Uhrich, *J. Biomed. Mater. Res., Part A* **2005**, *72A*, 354.
[57] I. Pountos, T. Georgouli, G. M. Calori, P. V. Giannoudis, *Sci. World J.* **2012**, *2012*, 606404.
[58] B. Humbert, M. Alnot, F. Quilès, *Spectrochim. Acta, Part A* **1998**, *54*, 465.
[59] W. A. Lackington, L. Fleyshman, P. Schweizer, Y. Elbs-Glatz, S. Guimond, M. Rottmar, *Mater. Today Bio* **2022**, *15*, 100303.
[60] F. M. Watt, *EMBO J.* **2002**, *21*, 3919.
[61] J. P. Kim, K. Zhang, J. D. Chen, R. H. Kramer, D. T. Woodley, *J. Biol. Chem.* **1994**, *269*, 26926.
[62] M. Pranskunas, L. Poskevicius, G. Juodzbalys, R. Kubilius, R. Jimbo, *J. Oral Maxillofac. Res.* **2016**, *7*, e2.